

# Effects of simulated cosmological magnetic fields on the galaxy population

Federico Marinacci<sup>\*</sup> and Mark Vogelsberger

*Kavli Institute for Astrophysics and Space Research, Massachusetts Institute of Technology, Cambridge, MA 02139, USA*

Accepted 2015 November 7. Received 2015 October 17; in original form 2015 August 26.

## ABSTRACT

We investigate the effects of varying the intensity of the primordial magnetic seed field on the global properties of the galaxy population in ideal magnetohydrodynamic cosmological simulations performed with the moving-mesh code AREPO. We vary the seed field in our calculations in a range of values still compatible with the current cosmological upper limits. We show that above a critical intensity of  $\simeq 10^{-9}$  G, the additional pressure arising from the field strongly affects the evolution of gaseous structures, leading to a suppression of the cosmic star formation history, which is stronger for larger seed fields. This directly reflects into a lower total galaxy count above a fixed stellar mass threshold at all redshifts, and a lower galaxy number density at fixed stellar mass and a less massive stellar component at fixed virial mass at all mass scales. These signatures may be used, in addition to the existing methods, to derive tighter constraints on primordial magnetic seed field intensities.

**Key words:** – magnetic fields – MHD – galaxies: general – cosmology: theory.

## 1 INTRODUCTION

Much progress has been made to understand the evolution of magnetic fields in the cosmological context, and especially on investigating mechanisms through which B fields are set to their present-day strength in galaxies and galaxy clusters. Although there are strong indications that dynamo processes play a crucial role in amplifying pre-existing B fields (Hanasz et al. 2009; Schober et al. 2013), the origin of these seed fields still remains uncertain. In particular, it is unclear whether these seeds are of cosmological origin, i.e. produced at shocks (Ryu et al. 1998) or during inflation and phase transitions in the early Universe (Widrow et al. 2012), or generated by stars in proto-galaxies (Schleicher et al. 2010) and subsequently ejected by galactic winds (Völk & Atoyan 2000) and active galactic nucleus activity (Furlanetto & Loeb 2001).

It is intrinsically difficult to observe magnetic fields outside haloes or at high redshift with the current generation of instruments (Beck 2007). The detection of magnetic fields outside collapsed structures is particularly challenging because the expected intensities ( $\lesssim 1$  nG) are well below the ones observed in galaxies and galaxy clusters ( $\sim 1 \mu\text{G}$ ). Hence, most of the constraints on primordial magnetic fields are upper limits. These are in turn derived by considering how the predicted effect of such seed fields would compare to

actual observations of more well-determined quantities such as the cosmic microwave background power spectrum or polarization (Barrow et al. 1997; Durrer et al. 2000; Jedamzik et al. 2000; Kahniashvili et al. 2009, 2010; Planck Collaboration XIX 2015), the isotropy in the distribution of ultrahigh energy cosmic rays (e.g. Lee et al. 1995), Big bang nucleosynthesis abundances (Grasso & Rubinstein 1995, 2001), Faraday rotation measure, Ly  $\alpha$  forest and Sunyaev–Zel’dovich effect statistics (Blasi et al. 1999; Shaw & Lewis 2012). Interestingly, most of the limits converge towards a maximum present-day field strength of  $\sim 1 - 10$  nG. Moreover, possible lower limits ( $\gtrsim 10^{-15}$  G) have been inferred from  $\gamma$ -ray and TeV blazars observations (Neronov & Semikoz 2009; Neronov & Vovk 2010).

In this Letter, we examine how strong the effects of cosmological B fields (i.e. fields generated in the early Universe) on the global properties of the galaxy population are as a function of the field strength, and determine what is the critical intensity at which they become noticeable. We run a set of cosmological magnetohydrodynamic (MHD) simulations with varying seed field intensities and study the changes in the cosmic star formation density, stellar mass function, stellar-to-halo mass relation, the evolution of the mean magnetic field and total galaxy number. The Letter is organized as follows. In Section 2, we present analytic considerations to relate the seed field used in our runs to the current upper limits and we estimate at what intensity those fields are expected to significantly impact the dynamics of the gas.

<sup>\*</sup> E-mail: fmarinac@mit.edu

We introduce the setup of our simulations in Section 3 and we describe the main results of our analysis in Section 4. Finally, we draw our conclusions in Section 5.

## 2 ANALYTIC CONSIDERATIONS

In our simulations, the initial seed magnetic field is uniform and threads the computational domain along a predefined direction (see also Sect. 3). However, in the majority of earlier work, upper limits for cosmological magnetic fields are inferred by assuming that those fields are described by a power spectrum of the form (see e.g. Kahniashvili et al. 2009)

$$P_B(k) = A_B k^{n_B} \quad k < k_D, \quad (1)$$

where  $A_B$  is a normalization constant,  $n_B$  is the spectral index and  $k_D$  is the so-called Alfvén damping scale (Jedamzik et al. 1998) above which it is assumed that no power is present. Therefore, it is important to establish a direct connection between the uniform field intensities used in this work and those derived through equation (1). Before proceeding, we note that the value of  $n_B$  is uncertain (usually  $-3 < n_B \leq 2$ ; Kahniashvili et al. 2010) and can have a significant impact on the value of the inferred intensities of cosmological B fields. It is also to avoid this additional source of uncertainty that we opted for the simpler uniform field setup in our runs.

The information about the intensity of cosmological seed B fields is contained in the normalization constant  $A_B$ , which is linked to a smoothed comoving field amplitude on a comoving scale  $\lambda$  via a convolution with a Gaussian kernel through (Planck Collaboration XIX 2015)

$$B_\lambda^2 = \int_0^{+\infty} \frac{dk k^2}{2\pi^2} e^{-k^2 \lambda^2} P_B(k) = \frac{|A_B|}{4\pi^2 \lambda^{n_B+3}} \Gamma\left(\frac{n_B+3}{2}\right), \quad (2)$$

where  $\Gamma$  is Euler’s gamma function. From equation (2) it is easy to connect the smoothed field amplitude at two arbitrary scales  $\lambda_1$  and  $\lambda_2$  as

$$B_{\lambda_2} = B_{\lambda_1} \left(\frac{\lambda_1}{\lambda_2}\right)^{\frac{n_B+3}{2}}. \quad (3)$$

In our simulation setup, the initial seed field is coherent on a  $25 h^{-1} \text{Mpc} \simeq 37 \text{Mpc}$  scale. Hence, a smoothed field  $B_{1 \text{Mpc}} = 1 \text{nG}$  – a representative value of current upper limits (Planck Collaboration XIX 2015) – translates into  $B_{37 \text{Mpc}} \simeq 1.2 \times 10^{-4} \text{nG}$  for  $n_B = 2$ , and  $B_{37 \text{Mpc}} \simeq 0.84 \text{nG}$  for  $n_B = -2.9$ .

A more physically motivated way to express the intensity of a magnetic seed field whose power spectrum satisfies equation (1) is to replace  $B_\lambda$  with the *effective* field containing the same magnetic energy density as the one obtained by integrating the power spectrum over all scales. In this way, the information at all spatial scales is used and the resulting field intensity can be compared in a more meaningful way to the uniform seed field that we have adopted in our calculations. The effective field is defined as (Kahniashvili et al. 2010, equation 5)

$$B_{\text{eff}} = \frac{B_\lambda(k_D \lambda)^{(n_B+3)/2}}{\Gamma^{1/2}(n_B/2 + 5/2)}. \quad (4)$$

By applying equation (4) in the case of the  $n_B$  interval that we have examined above, we obtain an effective field  $B_{\text{eff}} \simeq 1.22 \text{nG}$  and  $B_{\text{eff}} \simeq 240 \text{nG}$  for  $n_B = -2.9$  and  $n_B = 2$ , respectively. These values have been derived for  $B_{1 \text{Mpc}} = 1 \text{nG}$  and by adopting the expression for  $k_D$  given in equation (3) of Planck Collaboration XIX (2015). The maximum seed field value that we employ in our simulations is consistent with those limits.

As we mentioned in the Introduction, the majority of the currently available upper limits translate into effective seed fields with intensities of the order of  $1 - 10 \text{nG}$ . We now present two simple arguments showing that significant effects on the evolution of the galaxy population must be expected if the Universe is permeated by those (or stronger) fields. We start by noting that in ideal MHD, the magnetic field flux is conserved. This leads to the scaling relation (Grasso & Rubinstein 2001)

$$\|\mathbf{B}_{\text{gal}}\| = 10 \left(\frac{\|\mathbf{B}_0\|}{1 \text{nG}}\right) \left(\frac{\delta}{10^6}\right)^{2/3} \mu\text{G}, \quad (5)$$

where  $\mathbf{B}_0$  is the intensity of the initial seed field and  $\delta$  is the density contrast between the average gas density within galaxies and that in the intergalactic space. Equation (5) states that the final field intensity observed nowadays in galaxies ( $\sim$  a few  $\mu\text{G}$ ) can be entirely accounted for by adiabatic compression of an initial seed field of  $1 \text{nG}$ . However, several numerical studies (see Marinacci et al. 2015, and references therein) have shown that additional processes, such as small-scale dynamo and turbulent or shearing flows, play a key role in amplifying the magnetic field to its final strength. It is thus plausible to assume that seed fields of  $\sim 1 \text{nG}$  would be over-amplified by the presence of these (small-scale) mechanisms. This over-amplification would in turn leave its imprint on galactic properties by enhancing the dynamical role of magnetic fields.

Magnetic fields start to play a role in the gas dynamics if the magnetic pressure becomes comparable to the thermal gas pressure, viz.

$$\|\mathbf{B}\|^2 \gtrsim 8\pi\rho \frac{kT}{\mu m_p}, \quad (6)$$

where  $\|\mathbf{B}\|$  is the magnetic field intensity  $\rho$  and  $T$  the gas density and temperature,  $k$  the Boltzmann constant,  $\mu$  the gas mean molecular weight and  $m_p$  the proton mass. By considering a fully-ionized gas of primordial composition ( $X = 0.76$ ), we can rewrite equation (6) in terms of the comoving magnetic field intensity as

$$\|\mathbf{B}\| \gtrsim 5.61 \left(\frac{\Omega_b h^2}{0.022}\right)^{1/2} \left(\frac{T}{10^4 \text{K}}\right)^{1/2} (1+z)^{-1/2} \text{nG}, \quad (7)$$

where  $h = H_0/100 \text{km s}^{-1} \text{Mpc}^{-1}$ ,  $\Omega_b$  is the baryon density and  $z$  the redshift.

Equation (7) shows that the transition to magnetically dominated gas flows occurs at a critical seed magnetic field strength between  $1$  and  $10 \text{nG}$ , in line with the estimates and the observational constraints discussed earlier. In particular, in our runs the gas reaches temperatures of  $\simeq 10^4 \text{K}$  at the end of the reionization, which occurs at  $z_{\text{reion}} = 6$  for our choice of the UV background (Faucher-Giguère et al. 2009). This implies a critical seed B field  $\|\mathbf{B}\| \gtrsim 1.44 \text{nG}$ . Therefore, we anticipate a significant effect on galactic evolutionary processes at these B field intensities.

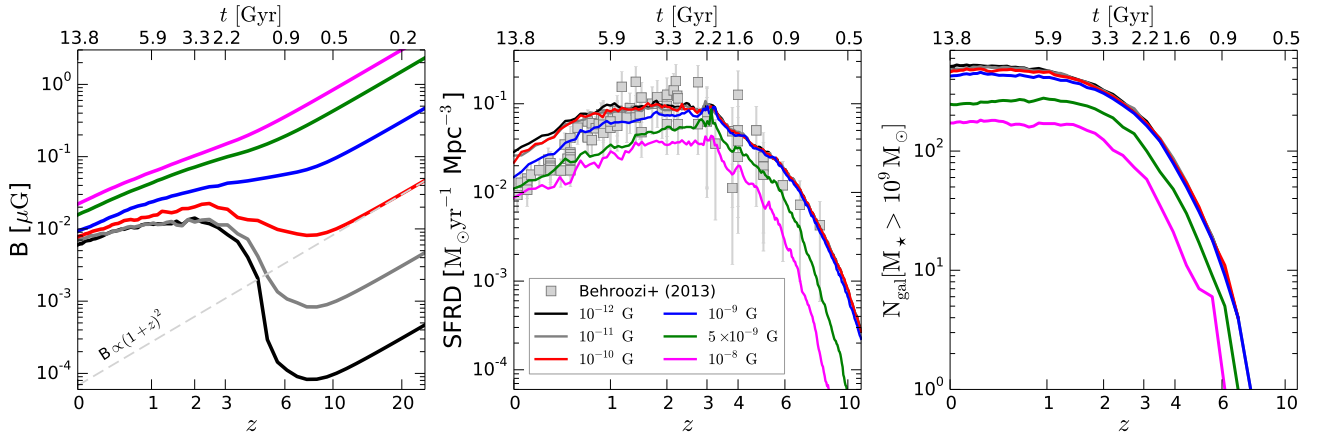


**Figure 1.** Left: evolution of the volume-weighted rms B field strength. Above the critical B field value of  $10^{-9}$  G the field intensity is set by flux conservation and little turbulent amplification is present. Centre: evolution of the cosmic star formation rate density (SFRD) together with a compilation of observational data taken from Behroozi et al. (2013). For larger seed magnetic field strengths there is an increasing suppression of the SFRD, which is present at all times for seed fields  $> 10^{-9}$  G. Right: evolution of the total galaxy number above a stellar mass threshold of  $10^9 M_{\odot}$ . The decrease in the total number of objects for seed field  $> 10^{-9}$  G is visible at all times.

### 3 SIMULATIONS SETUP

Our simulations evolve a uniformly sampled box from the initial redshift  $z = 127$  to the present day. We adopt a  $\Lambda$  cold dark matter cosmology with parameters  $\Omega_m = 0.302$ ,  $\Omega_b = 0.04751$ ,  $\Omega_{\Lambda} = 0.698$ ,  $\sigma_8 = 0.817$ ,  $n_s = 0.9671$ , and  $H_0 = 68 \text{ km s}^{-1} \text{Mpc}^{-1}$  derived by an independent re-analysis of *Planck* data by Spergel et al. (2015). All the runs are performed with the moving-mesh code AREPO (Springel 2010), together with a module for ideal MHD (Pakmor & Springel 2013) based on the 8-wave Powell et al. (1999) formalism to control divergence errors. The code is complemented with a galaxy formation physics model developed for the ILLUSTRIS simulation suite (Vogelsberger et al. 2014), which includes as major components: (1) primordial and metal-line cooling with self-shielding corrections (Rahmati et al. 2013), (2) an updated version of the Springel & Hernquist (2003) model for star formation with a Chabrier (2003) initial mass function, (3) stellar evolution, gas recycling and chemical enrichment, (4) a kinetic galactic wind scheme in which the wind speed is determined by the local dark matter velocity dispersion in haloes (see e.g. Puchwein & Springel 2013), (5) black hole seeding, accretion, merging and feedback (see also Springel et al. 2005). In this work we use the fiducial settings of the model presented in Vogelsberger et al. (2013).

We sample a  $25 \text{ h}^{-1} \text{Mpc}$  box size with  $2 \times 256^3$  resolution elements. Magnetic fields are added at the beginning of the calculation as a uniform seed field throughout the box. We choose this initial setup because it is the simplest divergence-free configuration to implement and has also the advantage that the field is specified once its intensity is fixed (but see Marinacci et al. 2015, for a discussion on how the initial field direction affects its properties). We keep the direction of the field fixed in all simulations along the  $z$ -axis, but change the (comoving) strength of the initial seed in the interval  $[10^{-12} - 10^{-8}] \text{ G}$ .

### 4 RESULTS

The left-hand panel of Fig. 1 presents the time evolution of the (volume-weighted) rms B field intensity as a function of redshift. The initial seed field intensity is indicated in the legend. At low seed fields ( $< 10^{-9}$  G), after a first phase dominated by the expansion of the Universe, in which the B field strength declines  $\propto (1+z)^2$  (grey dashed line), there is an upturn of the mean B field intensity at  $z \approx 6$ , after which the field is amplified by structure formation. The amplification saturates quickly, leaving behind an average field of  $\sim 10^{-2} \mu\text{G}$ , whose amplitude slowly declines with time. The situation is different for seed fields  $\geq 10^{-9}$  G. In those cases, the amplification of the field due to build-up of cosmic structures is less prominent. Indeed, the magnetic field strength steadily drops with time and adiabatic compression alone is largely sufficient to set the B field intensities observed in the present-day Universe (see eq. [5]).

The increased magnetic field strength for large seed fields implies a larger magnetic pressure acting on the gas, which in turn provides more support against gravitational collapse, potentially affecting the efficiency of its conversion into stars. We illustrate this in the central panel of Fig. 1 in which we show the cosmic star formation rate density (SFRD) as a function of redshift compared to a compilation of observational determinations taken from Behroozi et al. (2013). We can roughly divide the simulation set in two groups, depending on whether the initial seed field is below or above the critical value of  $10^{-9}$  G, which is very close to the one that we have determined analytically. Below this value, the magnetic field is still dynamically negligible (see eq. [7]) and the effects on the SFRD are minimal. Conversely, seed fields  $\geq 10^{-9}$  G have a significant impact on gas dynamics. The result is a noticeable reduction of the global SFRD, which is more prominent the larger the seed field and increasingly falls short of the observational findings especially at the star formation peak at  $z \sim 2$ , while reconciling the simulations to the observed level of star formation at  $z \simeq 0$ . The simulation with seed field  $10^{-9}$  G exhibits an intermediate behaviour. At  $z \gtrsim 3$ , it follows very closely the

same trend of the simulations with a lower seed field. A reduction in the SFRD (about a factor of 2 with respect to the runs with seed field  $< 10^{-9}$  G) only occurs after  $z \sim 3$ .

The right-hand panel of Fig. 1 displays the evolution of the total number of galaxy above a stellar mass threshold of  $10^9 M_\odot$ . The stellar mass is determined as the mass in stars contained within *twice* the stellar half-mass radius of each object. From the plot, it can be readily appreciated that the number of galaxies grows very rapidly for  $z \lesssim 6$  and by  $z \simeq 2$  (approximately at the peak of the cosmic SFRD) already a significant fraction ( $\gtrsim 60\%$ ) of the total objects has formed. The suppression of the cosmic SFRD due to increasing B seed fields intensities translates into a decrease of the total number of galaxy formed. The decrease is more pronounced for larger B field strengths and particularly noticeable for all the runs with fields above the critical intensities value of  $10^{-9}$  G. In those cases, the deficiency in the total galaxy number relative to simulations with seed field strengths below the critical value – which closely track one another – is present at all redshifts. Again, the  $10^{-9}$  G simulation shows an intermediate behaviour starting to slightly deviate from the trend followed by lower seed field runs only after  $z \simeq 2$ . We explicitly checked that the general trends discussed above are roughly independent from the particular value of the stellar mass cut adopted, at least up to  $10^{10} M_\odot$  where minor differences in the final total number of objects formed start to be present also in runs with seed field intensities  $< 10^{-9}$  G.

The top panel of Fig. 2 shows the redshift zero galaxy stellar mass function for all simulations together with observational values inferred from SDSS data (Bernardi et al. 2013). Due to the inability of small haloes to accrete highly magnetized gas, we expect a global reduction of the number of galaxy per unit stellar mass for increasing seed field intensities. The plot fully confirms these expectations and shows that the effect is stronger the larger the initial seed field. For seed fields  $\leq 10^{-9}$  G, the mass functions agree, within the scatter, over all the considered mass range. For seed fields above  $10^{-9}$  G, the reduction in number density is clearly visible up to  $M_\star \sim 10^{10.5} M_\odot$ , where the number of galaxies is underpredicted compared to the observations. At a stellar mass of  $\sim 10^{10.5} M_\odot$ , the discrepancy among the different runs is less prominent, an effect likely due to the fact that these haloes are massive enough to power their star formation even in the presence of a high B field. For larger  $M_\star$  (up to  $\sim 10^{11.5} M_\odot$ ) the differences grow again, signalling that the building blocks of these large structures, which accrete a significant fraction of their mass through mergers, contain on average less stars for large seed fields.

In the bottom panel of Fig. 2, we present the redshift zero stellar-to-halo mass relation as a function of the virial mass. For comparison, we also show the same relation derived via abundance matching (Behroozi et al. 2013). Again, the net effect of an increase of the seed field strength is a reduction of the ratio between stellar and halo mass over the whole range of virial masses in the simulations. The general division in two groups discussed previously can also be applied here. In particular, simulations with seed fields  $< 10^{-9}$  G track each other quite well, while for seed fields  $\geq 10^{-9}$  G, the stellar-to-halo mass ratio becomes smaller for increasing value of the initial seed magnetic field. At low halo masses, the conversion efficiency of gas into stars is consider-

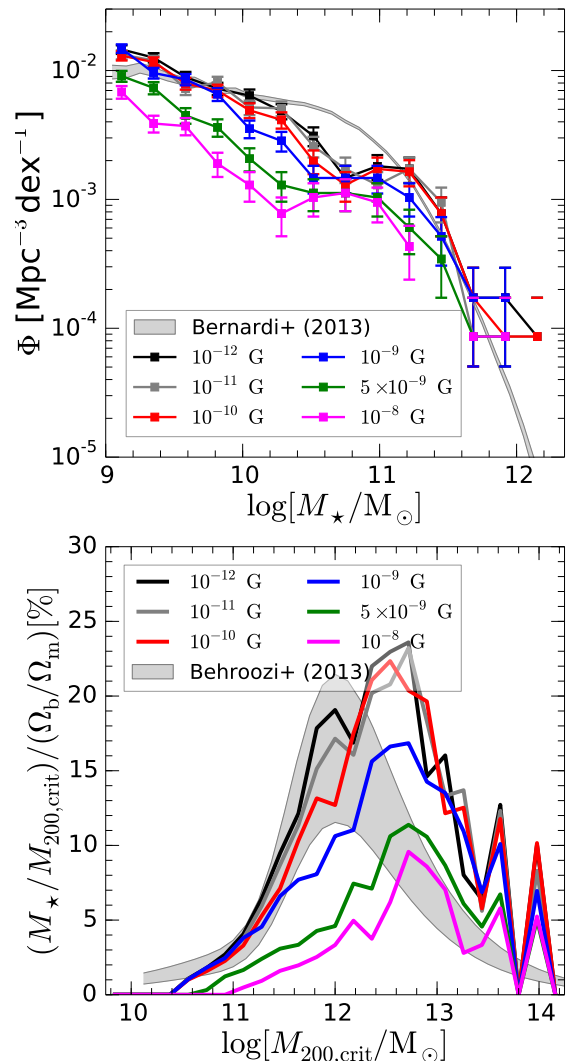


**Figure 2.** Top: galaxy stellar mass function compared to SDSS observations (Bernardi et al. 2013). The suppression of star formation causes a decrease of the number of objects at all mass scales. The effect is stronger for larger seed field intensities. Bottom: stellar-to-halo mass relation contrasted to the abundance matching predictions of Behroozi et al. (2013). At any given virial mass, the stellar content of haloes decreases for increasing seed B field strengths.

ably reduced for the highest seed magnetic fields, for which virial masses  $\gtrsim 10^{11} M_\odot$  are required on average for a halo to host stars. The maximum conversion efficiency is found for virial masses  $\sim 10^{12.5} M_\odot$ , about  $\simeq 0.5$  dex larger than the analogous relation found in ILLUSTRIS and inferred from abundance matching. Moreover, the peak of the relation appears to be shifting, albeit only slightly, towards large halo masses. At the high-mass end ( $M_{200, \text{crit}} \sim 10^{13.5} M_\odot$ ), the discrepancy among curves gets smaller, but the main trend with the seed magnetic field intensity is still present.

## 5 SUMMARY AND CONCLUSIONS

We have investigated how the presence of cosmological magnetic fields affects the global properties of the galaxy popula-

tion using cosmological MHD simulations. Our main results can be summarized as follows.

(i) For seed B fields  $\gtrsim 10^{-9}$  G, the increased magnetic pressure hampers gas accretion into low-mass dark matter haloes. This causes a reduction of the cosmic SFRD, which becomes more marked for increasing seed field intensities.

(ii) The suppression of the cosmic SFRD also results in a reduction of the total galaxy number at all redshifts and of present-day galaxy stellar mass function in all stellar mass bins and in particular for  $M_* \lesssim 10^{10} M_\odot$ . Again, this effect is stronger for larger seed B fields.

(iii) At fixed virial mass, haloes tend to contain significantly less stars for increasing seed field intensities. This is particularly evident for the less massive haloes. Indeed, for the largest seed field considered in the simulations, virial masses  $\gtrsim 10^{11} M_\odot$  are required for a halo to host stars.

Our simulations neglect any change that the presence of a seed magnetic field can induce on the initial matter power spectrum. Several authors (e.g. Sethi & Subramanian 2005, 2009; Yamazaki et al. 2006; Fedeli & Moscardini 2012) have argued that seed magnetic fields can affect the distribution of power especially at small/intermediate scales, at which the clustering of the matter would be enhanced. By not considering these variations to the matter power spectrum, we might overestimate the effect of large B seed field on small haloes in our runs. Moreover, our cosmological volume is fully magnetized at the initial redshift, which again may reinforce the effects of B fields on the gas with respect to a scenario in which the field is first generated within galaxies and then ejected in the intergalactic space.

Another point to bear in mind is that degree of reduction of the stellar content and star formation in haloes might also depend on the choice of the feedback model adopted in the simulations. The fiducial ILLUSTRIS feedback model used in our runs is at the upper end of what is energetically plausible, in particular for the generation of galactic winds. Therefore, it is conceivable that (strong) seed magnetic fields would cause a smaller suppression of the star formation rate and galaxy stellar masses with less efficient feedback loops, helping to alleviate some of the tensions with the observations that we have discussed.

Even with these caveats, from our runs emerges a consistent picture in which primordial magnetic seed fields and galaxy properties are closely related. In particular, primordial seed magnetic fields compatible with the currently available upper limits leave detectable signatures on global properties of the galaxy population, which can potentially be exploited, in conjunction with the existing methods, to put tighter constraints on their intensities.

## ACKNOWLEDGEMENTS

We thank an anonymous referee for a constructive report and Lars Hernquist, Philip Mocz, Ruediger Pakmor, David Spergel, Volker Springel and Paul Torrey for their insightful comments. We further thank Volker Springel for giving us access to AREPO. MV acknowledges support through an MIT RSC award. The simulations were performed on the joint MIT-Harvard computing cluster supported by MKI

and FAS. All the figures were created with MATPLOTLIB (Hunter 2007).

## REFERENCES

- Barrow J. D., Ferreira P. G., Silk J., 1997, *Phys. Rev. Lett.*, **78**, 3610
- Beck R., 2007, *Adv. Radio Sci.*, **5**, 399
- Behroozi P. S., Wechsler R. H., Conroy C., 2013, *ApJ*, **770**, 57
- Bernardi M., Meert A., Sheth R. K., Vikram V., Huertas-Company M., Mei S., Shankar F., 2013, *MNRAS*, **436**, 697
- Blasi P., Burles S., Olinto A. V., 1999, *ApJ*, **514**, L79
- Chabrier G., 2003, *ApJ*, **586**, L133
- Durrer R., Ferreira P. G., Kahnishvili T., 2000, *Phys. Rev. D*, **61**, 043001
- Faucher-Giguère C.-A., Lidz A., Zaldarriaga M., Hernquist L., 2009, *ApJ*, **703**, 1416
- Fedeli C., Moscardini L., 2012, *J. Cosmol. Astropart. Phys.*, **11**, 55
- Furlanetto S. R., Loeb A., 2001, *ApJ*, **556**, 619
- Grasso D., Rubinstein H. R., 1995, *Astropart. Phys.*, **3**, 95
- Grasso D., Rubinstein H. R., 2001, *Phys. Rep.*, **348**, 163
- Hanasz M., Wóltański D., Kowalik K., 2009, *ApJ*, **706**, L155
- Hunter J. D., 2007, *Comput. Sci. Eng.*, **9**, 90
- Jedamzik K., Katalinić V., Olinto A. V., 1998, *Phys. Rev. D*, **57**, 3264
- Jedamzik K., Katalinić V., Olinto A. V., 2000, *Physical Review Letters*, **85**, 700
- Kahnishvili T., Maravin Y., Kosowsky A., 2009, *Phys. Rev. D*, **80**, 023009
- Kahnishvili T., Tevzadze A. G., Sethi S. K., Pandey K., Ratna B., 2010, *Phys. Rev. D*, **82**, 083005
- Lee S., Olinto A. V., Sigl G., 1995, *ApJ*, **455**, L21
- Marinacci F., Vogelsberger M., Mocz P., Pakmor R., 2015, *MNRAS*, **453**, 3999
- Neronov A., Semikoz D. V., 2009, *Phys. Rev. D*, **80**, 123012
- Neronov A., Vovk I., 2010, *Science*, **328**, 73
- Pakmor R., Springel V., 2013, *MNRAS*, **432**, 176
- Planck Collaboration XIX, 2015, preprint, ([arXiv:1502.01594](https://arxiv.org/abs/1502.01594))
- Powell K. G., Roe P. L., Linde T. J., Gombosi T. I., De Zeeuw D. L., 1999, *J. Comput. Phys.*, **154**, 284
- Puchwein E., Springel V., 2013, *MNRAS*, **428**, 2966
- Rahmati A., Pawlik A. H., Raičević M., Schaye J., 2013, *MNRAS*, **430**, 2427
- Ryu D., Kang H., Biermann P. L., 1998, *A&A*, **335**, 19
- Schleicher D. R. G., Banerjee R., Sur S., Arshakian T. G., Klessen R. S., Beck R., Spaans M., 2010, *A&A*, **522**, A115
- Schober J., Schleicher D. R. G., Klessen R. S., 2013, *A&A*, **560**, A87
- Sethi S. K., Subramanian K., 2005, *MNRAS*, **356**, 778
- Sethi S. K., Subramanian K., 2009, *J. Cosmol. Astropart. Phys.*, **11**, 21
- Shaw J. R., Lewis A., 2012, *Phys. Rev. D*, **86**, 043510
- Spergel D. N., Flauger R., Hložek R., 2015, *Phys. Rev. D*, **91**, 023518
- Springel V., 2010, *MNRAS*, **401**, 791
- Springel V., Hernquist L., 2003, *MNRAS*, **339**, 289
- Springel V., Di Matteo T., Hernquist L., 2005, *MNRAS*, **361**, 776
- Vogelsberger M., Genel S., Sijacki D., Torrey P., Springel V., Hernquist L., 2013, *MNRAS*, **436**, 3031
- Vogelsberger M., et al., 2014, *MNRAS*, **444**, 1518
- Völk H. J., Atayan A. M., 2000, *ApJ*, **541**, 88
- Widrow L. M., Ryu D., Schleicher D. R. G., Subramanian K., Tsagas C. G., Treumann R. A., 2012, *Space Sci. Rev.*, **166**, 37
- Yamazaki D. G., Ichiki K., Umezu K.-I., Hanayama H., 2006, *Phys. Rev. D*, **74**, 123518